Gradient Descent-Based Direction-of-Arrival Estimation for Lens Antenna Array

Trong-Dai Hoang, Xiaojing Huang, *Senior Member, IEEE*, and Peiyuan Qin, *Senior Member, IEEE*

***Abstract*—In this letter, we investigate a novel optimization approach to direction-of-arrival (DoA) estimation for a lens antenna array. Inspired by a property of the sinc function and ℓ_2-norm optimization, we develop the gradient descent-based spatial spectrum reconstruction (GD-SSR) to estimate the DoAs based on the sum signal covariance vector (SSCV). Our proposed algorithm does not require a priori knowledge of signal number and has a lower complexity compared with existing techniques while achieving a better estimation performance, even in a low-SNR regime. In addition, the proposed model does not require any pretraining process as prior learning-based methods. The simulation results show that our scheme not only outperforms other techniques but also resolves the angular ambiguity problem.**

***Index Terms*—Direction-of-arrival (DoA), lens antenna array, gradient descent (GD), spatial spectrum reconstruction (SSR).**

I. Introduction

THE lens antenna array (LAA) is one of the cost-effective array designs for millimeter wave (mmWave) communications to achieve high gains with a limited number of radio frequency (RF) chains [1]. Generally, a lens is employed as a passive beamforming device replacing a heavy network of phase shifters in a hybrid precoding system, while the required directivity can be achieved based on the energy-focusing property. In other words, the incoming signals from different directions have energy distributed across the antenna elements of LAA [2]. Smaller subgroups of the entire array are then distinguished and connected to respective RF chains for further processing. It is worth noting that estimating the direction-of-arrival (DoA) of the received signal is crucial to identify the beam from a mobile user before establishing a connection in the access channel using an LAA.

Various schemes have been investigated for DoA estimation and they can be classified into the following categories: subspace-fitting algorithms [3], [4], [5], compressed-sensing schemes [6], [7], and deep learning (DL)-aided estimators [8], [9]. Compared with other algorithms, subspace-based methods such as conventional multiple signal classification (C-MUSIC) can achieve a more satisfactory estimation performance. Inspired by another classical scheme for off-grid DoA estimation with a uniform linear array (ULA), known as the root-MUSIC (R-MUSIC) algorithm [4], a modified root-MUSIC (M-MUSIC) method in [5] can work with an LAA. In [5], Ni et al. propose a three-stage algorithm combining the root-finding step, outlier detection based on calculating the local outlier factor, and clustering the resulting DoA data points together. However, the M-MUSIC poses a remarkable computational burden for solving numerous high-order polynomial equations. In addition, as a common drawback in the MUSIC family, the number of received signals must be known as a prerequisite [2], [10]. Unlike subspace-based schemes, the compressed-sensing methods [6], [11] solve the DoA problem without a priori knowledge of signal number. Orthogonal matching pursuit (OMP) is a novel technique in this class due to its fast recovery speed and lower complexity [11]. OMP-based DoA estimation aims to reconstruct a spatial spectrum thanks to the sparsity of nonzero values in the angle space. Nevertheless, the OMP-aided recovered signal contains noise elements that deteriorate the estimation performance [2]. Moreover, the implementation of Cholesky or QR factorizations to find the least square solution in an individual OMP iteration requires a substantially high complexity [12].

In recent years, some learning architectures have been proposed to deal with the DoA problem [8], [9]. The multiple signal classification via DL (DeepMUSIC) has been introduced in [9] for multi-DoA estimation with superior accuracy compared to subspace-based algorithms. The DeepMUSIC is considered as a system of parallel multiple convolutional neural networks (CNNs), each of which reconstructs a subregion of the angular spectrum. Despite the above improvements, those CNNs with numerous learning parameters require remarkable computation in training and practical deployment. The authors in [8] have presented a lower-complexity scheme, namely root-spectrum network (RSNet), by replacing those CNNs in DeepMUSIC with feedforward neural networks but still guaranteeing an enhanced performance. However, the above methods are supervised-learning frameworks in which large-scale pre-trained models with huge learning parameters must be optimized and stored in a core station. This requires a massive computational resource. To solve the above-mentioned problems, we propose the gradient descent (GD)-based spatial spectrum reconstruction (GD-SSR) method in this letter. Our GD-SSR employs a GD algorithm which is commonly used to train DL models [9], [13], [14], [15], [16]. Different from the existing deep networks, the GD-SSR does not require any training phase. Furthermore, our method takes advantage of the sinc function in the LAA's array response to obtain the sum signal covariance vector (SSCV). By utilizing the SSCV, the GD-SSR can recover the target spectrum without prior knowledge of the incoming signal number. We also derive the number of floating-point operations (FLOPs) [17] of GD-SSR and show that it has lower computational complexity than

Manuscript received 20 May 2023; revised 30 June 2023; accepted 1 July 2023. Date of publication 5 July 2023; date of current version 13 July 2023. This work was supported by Australian Research Council Discovery Project under Grant DP220101158. The associate editor coordinating the review of this manuscript and approving it for publication was Dr. Lu Gan. *(Corresponding author: Trong-Dai Hoang.)*

The authors are with the Global Big Data Technologies Centre, University of Technology Sydney, Ultimo, NSW 2007, Australia (e-mail: dai.t.hoang@student.uts.edu.au; xiaojing.huang@uts.edu.au; peiyuan.qin@uts.edu.au).

Digital Object Identifier 10.1109/LSP.2023.3292742

the existing algorithms. The simulation results show our proposed method not only improves the estimation performance but also resolves the angle ambiguity problem, even in a low-SNR regime.

Notations: The superscripts $(\cdot)^*$, $(\cdot)^T$, and $(\cdot)^H$ denote the conjugate, transpose, and conjugate transpose of a complex vector or matrix, respectively. The notation a_m represents the mth element of a vector $\mathbf{a}$. Additionally, the mth column or row of a matrix $\mathbf{A}$ are denoted by $\mathbf{A}_{:,m}$ or $\mathbf{A}_{m,:}$, respectively. The notation $\mathbb{E}\{\cdot\}$ represents the expectation of a random variable. $\mathbf{I}_M$ denotes an $M \times M$ matrix with ones on the main diagonal and zeros elsewhere. The operator $\mathrm{diag}\{\cdot\}$ with the vector argument inside creates a square matrix that contains all elements of that vector on its main diagonal and has zeros elsewhere. The operator $\circ$ denotes the Hadamard product.

II. System Model

We assume that P narrowband far-field signals, which are from distinct directions θ_p, where $p = 1, 2, \ldots, P$, impinge upon an LAA composed of M antennas placed on the focal arc of the lens. Let the central antenna be the reference element. With the center of the LAA placed at the origin, the antennas can be indexed as $-\overline{M}, \ldots, 0, \ldots, \overline{M}$, where $\overline{M} = \lfloor (M-1)/2 \rfloor$ is the half number of antennas. At the receiver, a $D_y \times D_z$ EM lens is placed on the y–z plane and the thickness of this lens is assumed to be negligible compared with its focal length. Let m denote the index of the antenna such that $m \in [-\overline{M}, \overline{M}]$. Then, the angular resolution of the lens is computed as $\sin\phi_m = m\lambda/D_y = m/\mathcal{D}$, where λ is the carrier wavelength, $\mathcal{D} \triangleq D_y/\lambda$ symbolizes the lens dimension along the azimuth plane normalized by signal wavelength, and ϕ_m represents the angular position of the mth antenna on the y axis. Without loss of generality, we assume that $\overline{M} = \lfloor \mathcal{D} \rfloor$.

According to [1], the array response of the mth antenna to a signal coming from direction θ can be expressed as

$$a_m(\theta) = \sqrt{\kappa}\,\mathrm{sinc}\left(m - \mathcal{D}\sin\theta\right), \tag{1}$$

where $\kappa \triangleq D_y D_z/\lambda^2$ is the normalized effective aperture. The received signal $x_m(t)$ at the mth antenna at time t over T uniquely spaced time snapshots is given as $x_m(t) = \sum_{p=1}^{P} s_p(t) a_m(\theta_p) + n_m(t)$, where $n_m(t)$ represents the zero-mean Gaussian noise at the mth antenna. In matrix form, the received signal $\mathbf{x}(t) = [x_{-\overline{M}}(t), \ldots, x_0(t), \ldots, x_{\overline{M}}(t)]^T \in \mathbb{C}^{M\times 1}$ can be modeled as

$$\mathbf{x}(t) = \mathbf{A}\mathbf{s}(t) + \mathbf{n}(t), \tag{2}$$

where $\mathbf{s}(t) = [s_1(t), \ldots, s_P(t)]^T \in \mathbb{C}^{P\times 1}$ denotes the signal vector, $\boldsymbol{\theta} = \{\theta_p\}_{p=1}^{P}$ contains signal directions, $\mathbf{A} = [\mathbf{a}(\theta_1), \ldots, \mathbf{a}(\theta_P)]^T \in \mathbb{R}^{M\times P}$ is the array manifold matrix with the pth column vector $\mathbf{a}(\theta_p) = [a_{-\overline{M}}(\theta_p), \ldots, a_0(\theta_p), \ldots, a_{\overline{M}}(\theta_p)]^T \in \mathbb{R}^{M\times 1}$, and $\mathbf{n}(t) = [n_{-\overline{M}}(t), \ldots, n_0(t), \ldots, n_{\overline{M}}(t)]^T \in \mathbb{C}^{M\times 1}$ represents the noise vector. Additionally, let $\sigma_{s,p}^2$, and σ_n^2 be the power of signal $s_p(t)$ and noise covariance, respectively. To simplify the DoA estimation, we assume that all incoming signals are independent and mutually uncorrelated. Furthermore, the signal vector $\mathbf{s}(t)$ and noise vector $\mathbf{n}(t)$ follow the circularly-symmetric jointly-Gaussian distributions $\mathcal{CN}(0, \mathbf{R}_S)$ and $\mathcal{CN}(0, \sigma_n^2\mathbf{I}_M)$, respectively. Based on the aforementioned assumptions, the signal power matrix is expressed as $\mathbf{R}_S = \mathrm{diag}\{[\sigma_{s,1}^2, \ldots, \sigma_{s,P}^2]^T\}$.

III. Proposed DoA Estimation Algorithm

A. Property of LAA

Based on the received signal shown in (2), the signal covariance matrix (SCM) is evaluated as

$$\mathbf{R} = \mathbb{E}\left\{\mathbf{x}(t)\mathbf{x}^H(t)\right\} = \mathbf{A}\overline{\mathbf{D}} + \sigma_n^2\mathbf{I}_M, \tag{3}$$

where $\overline{\mathbf{D}} \triangleq \mathbf{R}_S\mathbf{A}^T \in \mathbb{C}^{P\times M}$ is the pseudosignal matrix. The (p,m)th element $\bar{d}_{p,m}$ of $\overline{\mathbf{D}}$ is then computed as $\bar{d}_{p,m} = \sigma_{s,p}^2 a_m(\theta_p)$. Subsequently, we define $\overline{\mathbf{R}} \triangleq \mathbf{A}\overline{\mathbf{D}}$ and $\boldsymbol{\zeta}$, respectively, as the SCM in a noiseless environment and SSCV created by summing all column vectors of $\overline{\mathbf{R}}$. We can observe that the elements in vector $\boldsymbol{\zeta}$ are real values, $\boldsymbol{\zeta} \in \mathbb{R}^{M\times 1}$, as it can be evaluated as

$$\boldsymbol{\zeta} \triangleq \sum\nolimits_{m=-\overline{M}}^{\overline{M}} \overline{\mathbf{R}}_{:,m} = \mathbf{A}\mathbf{d}, \tag{4}$$

where the DoA profile vector $\mathbf{d}$ is defined as

$$\mathbf{d} \triangleq \sum\nolimits_{m=-\overline{M}}^{\overline{M}} \overline{\mathbf{D}}_{:,m} = \mathbf{R}_S\left(\sum\nolimits_{m=-\overline{M}}^{\overline{M}} \mathbf{A}_{m,:}\right)^T. \tag{5}$$

We note that σ_n^2 can be estimated as the minimum value among the entries $r_{m,m}$ on the diagonal of $\mathbf{R}$, as illustrated in [2, Eq. (6)]; thus, $\overline{\mathbf{R}}$ can be approximated as

$$\overline{\mathbf{R}} = \mathbf{R} - \sigma_n^2\mathbf{I}_M \approx \mathbf{R} - \left[\min\left(\{r_{m,m}\}_{m=-\overline{M}}^{\overline{M}}\right)\right]\mathbf{I}_M. \tag{6}$$

We subsequently consider the following feature.

Lemma 1: For a large-scale LAA system, i.e., $\overline{M} \to \infty$, the element in $\mathbf{d}$ corresponding to an incoming signal is a constant determined by the product of signal power and the normalized effective aperture.

Proof: Let $z \triangleq \mathcal{D}\sin\theta$, and $h(z) \triangleq \sum_{m=-\overline{M}}^{\overline{M}} \mathrm{sinc}(m-z)$ be the sum of all array responses to direction θ. We first consider the Fourier transform of $h(z)$ with respect to (w.r.t) z and note that $h(z)$ is a periodic signal with period 1. The Fourier coefficients ν_n can be calculated as

$$\begin{aligned}\nu_n &= \int_0^1 \sum\nolimits_{m=-\overline{M}}^{\overline{M}} \mathrm{sinc}\left(m-z\right) e^{-j2\pi nz} dz \\ &\overset{(a)}{=} \sum\nolimits_{m=-\infty}^{\infty} \left[\int_{m-1}^{m} \mathrm{sinc}(k) e^{j2\pi nk} dk\right] e^{-j2\pi nm} \\ &= \int_{-\infty}^{\infty} \mathrm{sinc}(k) e^{j2\pi nk} dk \overset{(b)}{=} \Pi(n).\end{aligned} \tag{7}$$

In (7), step (a) is achieved by assuming that $\overline{M} \to \infty$. In addition, equality (b) is obtained by observing that the left-hand-side term is the inverse Fourier transformation of the top-hat function $\Pi(n)$ given as [18, Ch. 5]

$$\Pi(n) = \begin{cases} 1 & |n| \lessgtr 1/2 \\ 0 & |n| \gtrless 1/2 \end{cases}. \tag{8}$$

Given (7) and (8), the corresponding Fourier series of $h(z)$ is then written as [18]

$$h(z) = \sum_{n=-\infty}^{\infty} \nu_n e^{-j2\pi nz} = 1. \tag{9}$$

Based on (1), (5) and (9), the pth element of $\mathbf{d} \in \mathbb{R}^{P\times 1}$ can be presented as $d_p = \sigma_{s,p}^2 \sum_{m=-\overline{M}}^{\overline{M}} a_m(\theta_p) = \sigma_{s,p}^2\sqrt{\kappa}$. This concludes the proof. ■

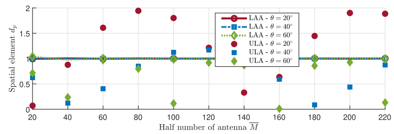

Fig. 1. Comparison between spatial elements d_p of LAA and ULA.

Fig. 1 visualizes the distribution of spatial elements in $\mathbf{d}$ of an LAA with $\kappa = 1$, compared to that of a ULA, in the case of $P = 3$ signals from directions $\boldsymbol{\theta} = \{20^\circ, 40^\circ, 60^\circ\}$, and the power coefficients are assumed as $\sigma_{s,1}^2 = \sigma_{s,2}^2 = \sigma_{s,3}^2 = 1$. It is shown that all elements d_p of the LAA converge to one value as $\overline{M}$ increases. On the other hand, the values of a ULA are not stable. For example, at $\overline{M} = 20$, the value representing $\theta = 20^\circ$ is approximately zero. This means that an element d_p may be ignored with a ULA. Thus, we can conclude that the property mentioned in Lemma 1 is unique for an LAA.

B. GD-Based DoA Estimation

Let $\theta_{\max}$, $\theta_{\min}$, and ρ be the maximum, minimum directions of incoming signals and resolution of DoA in the range of $[\theta_{\min}, \theta_{\max})$, respectively. The number of possible angles $\widetilde{P}$ is then computed as $\widetilde{P} = (\theta_{\max} - \theta_{\min})/\rho$. In addition, another way to interpret the system model in (4) is that the energy of received signals at the LAA antennas concentrates at few DoAs θ_p from all possible directions $\widetilde{\boldsymbol{\theta}} = \{\theta_p\}_{p=1}^{\widetilde{P}}$. In other words, the angles of incoming signals are sparse in the angular space. This motivates us to use a multilabel classification framework for spatial spectrum reconstruction. Let $\widetilde{\mathbf{d}} \in \mathbb{R}^{\widetilde{P}\times 1}$ be the spatial spectrum to be reconstructed. Based on Lemma 1, we can observe that the spectrum $\widetilde{\mathbf{d}}$ has high values at the indices of target DoAs and zeros elsewhere. Since we treat the DoA estimation as a multilabel classification, the sigmoid function $\mathcal{S}(x) = 1/(1+e^{-x})$ must be employed at the output of our algorithm to guarantee all the elements in $\widetilde{\mathbf{d}}$ always take values between 0 and 1. Thus, we define the output vector as $\widetilde{\mathbf{d}} \triangleq \mathcal{S}(\widehat{\mathbf{d}})$, where $\widehat{\mathbf{d}}$ is the vector of learning parameters.

We define $\boldsymbol{\Xi} = [\widetilde{\mathbf{a}}(\theta_1), \ldots, \widetilde{\mathbf{a}}(\theta_{\widetilde{P}})]$ as the measurement matrix containing $\widetilde{P}$ steering vectors $\widetilde{\mathbf{a}}(\theta_p) = [\widetilde{a}_{-\overline{M}}(\theta_p), \ldots, \widetilde{a}_0(\theta_p), \ldots, \widetilde{a}_{\overline{M}}(\theta_p)]^T \in \mathbb{R}^{M\times 1}$, and the mth element in $\widetilde{\mathbf{a}}(\theta_p)$ is designed as $\widetilde{a}_m(\theta_p) = \mathrm{sinc}(m - \mathcal{D}\sin\theta_p)$, which is different from (1). Finally, by treating the SSCV as the observed data, the SSR-inspired DoA estimation can be converted to attaining the ℓ_2-norm solution $\widetilde{\mathbf{d}}$ of the optimization problem given as

$$\widetilde{\mathbf{d}} = \underset{\widetilde{\mathbf{d}}}{\arg\min} \left\| \widetilde{\boldsymbol{\zeta}} - \boldsymbol{\Xi}\underline{\widetilde{\mathbf{d}}} \right\|_2^2, \tag{10}$$

where $\widetilde{\boldsymbol{\zeta}} \in \mathbb{R}^{M\times 1}$ is the normalized $\boldsymbol{\zeta}$. Let $\zeta_{\max}$ be the largest value of $\boldsymbol{\zeta}$, and it can be described as $\zeta_{\max} = \sqrt{\kappa}\sum_{p=1}^{P} a_{\underline{m}}(\theta_p)\sigma_{s,p}^2$, where $\underline{m} = \arg\min_m |m - \mathcal{D}\sin\theta_{\underline{p}}|$, and $\underline{p} = \arg\max_p(\{\sigma_{s,p}^2\}_{p=1}^P)$. Then the mth element of $\widetilde{\boldsymbol{\zeta}}$ can be computed as

$$\widetilde{\zeta}_m = \frac{\zeta_m}{\zeta_{\max}} = \sum_{p=1}^{P} \widetilde{a}_m(\theta_p)\frac{\sigma_{s,p}^2}{\widetilde{\zeta}_{\max}}, \tag{11}$$

Algorithm 1: GD-SSR-Aided DoA Estimation.

Input: $\{\mathbf{x}(t)\}_{t=1}^T$, $\boldsymbol{\Xi}$, $\mathcal{I}$, α, β_1, β_2, and ε.
Output: $\widetilde{\mathbf{d}}$.

1: Compute $\mathbf{R} = [\sum_{t=1}^T \mathbf{x}(t)\mathbf{x}^H(t)]/T$.
2: Obtain $\overline{\mathbf{R}}$ based on (6).
3: Compute $\boldsymbol{\zeta} = \sum_{m=-\overline{M}}^{\overline{M}} \overline{\mathbf{R}}_{:,m}$.
4: Obtain $\widetilde{\boldsymbol{\zeta}}$ based on (11).
5: Initialize $\widehat{\mathbf{d}}^{(0)}$, $\boldsymbol{\eta}^{(0)}$, and $\boldsymbol{\chi}^{(0)}$ as $\mathcal{P}\times 1$ vectors having random values.
7: **for** $i = 1$ to $\mathcal{I}$ **do**
8: Compute gradient vector $\boldsymbol{\mathcal{G}}^{(i)} = \partial\mathcal{L}(\widehat{\mathbf{d}}^{(i-1)}|\widetilde{\boldsymbol{\zeta}})/\partial\widehat{\mathbf{d}}$.
9: Update $\boldsymbol{\eta}^{(i)} = \beta_1\boldsymbol{\eta}^{(i-1)} + (1-\beta_1)\boldsymbol{\mathcal{G}}^{(i)}$.
10: Update $\boldsymbol{\chi}^{(i)} = \beta_2\boldsymbol{\chi}^{(i-1)} + (1-\beta_2)(\boldsymbol{\mathcal{G}}^{(i)})^2$.
11: Compute $\widehat{\boldsymbol{\eta}}^{(i)} = \boldsymbol{\eta}^{(i)}/(1-\beta_1^i)$.
12: Compute $\widehat{\boldsymbol{\chi}}^{(i)} = \boldsymbol{\chi}^{(i)}/(1-\beta_2^i)$.
13: Update $\widehat{\mathbf{d}}^{(i)} = \widehat{\mathbf{d}}^{(i-1)} - \alpha\widehat{\boldsymbol{\eta}}^{(i)}/(\sqrt{\widehat{\boldsymbol{\chi}}^{(i)}} + \varepsilon)$.
14: **end for**
15: Return estimated spatial spectrum $\widetilde{\mathbf{d}} = \mathcal{S}(\widehat{\mathbf{d}}^{(\mathcal{I})})$.

where $\widetilde{\zeta}_{\max} \triangleq \sum_{p=1}^{P} \widetilde{a}_{\underline{m}}(\theta_p)\sigma_{s,p}^2$. It can be observed from (10), and (11) that the pth element of $\widetilde{\mathbf{d}}$ is given as

$$\widetilde{d}_p = \sigma_{s,p}^2/\widetilde{\zeta}_{\max}. \tag{12}$$

Algorithm 1 summarizes the pseudocode of our GD-SSR for DoA estimation with an LAA. We note that $\mathbf{R}$ is obtained by averaging $\mathbf{x}(t)\mathbf{x}^H(t)$ after a finite number of snapshots in practice, as shown in Step 1. Steps 2–4 indicate how the normalized SSCV $\widetilde{\boldsymbol{\zeta}}$ is obtained. We note that Step 2 not only reduces the loss value and convergence time of GD but also ensures the overall effectiveness of the algorithm in a low-SNR regime. The remaining steps demonstrate the procedure of the GD algorithm. We employ the adaptive moment estimation (ADAM) optimization for its robustness toward sparse gradients and high-dimensional parameter spaces while maintaining a low complexity [19]. As shown in Steps 5–12, the solution $\tilde{\mathbf{d}}$ is estimated after $\mathcal{I}$ iterations of minimizing the mean-square-error (MSE) loss function [1], which is given by

$$\mathcal{L}\left(\widehat{\mathbf{d}}^{(i)}\middle|\widetilde{\boldsymbol{\zeta}}\right) = \left\|\widetilde{\boldsymbol{\zeta}} - \boldsymbol{\Xi}\mathcal{S}\left(\widehat{\mathbf{d}}^{(i)}\right)\right\|_2^2 = \left\|\widetilde{\boldsymbol{\zeta}} - \boldsymbol{\Xi}\widetilde{\mathbf{d}}^{(i)}\right\|_2^2, \tag{13}$$

where $\widetilde{\mathbf{d}}^{(i)} \triangleq \mathcal{S}(\widehat{\mathbf{d}}^{(i)})$ is the spectrum updated in the ith iteration. Based on (13), the gradient vector in the ith iteration is expressed as

$$\begin{aligned}\boldsymbol{\mathcal{G}}^{(i)} &= \frac{\partial\mathcal{L}\left(\widehat{\mathbf{d}}^{(i)}\middle|\widetilde{\boldsymbol{\zeta}}\right)}{\partial\widehat{\mathbf{d}}} = \frac{\partial\mathcal{L}\left(\widehat{\mathbf{d}}^{(i)}\middle|\widetilde{\boldsymbol{\zeta}}\right)}{\partial\widetilde{\mathbf{d}}^{(i)}}\cdot\frac{\partial\widetilde{\mathbf{d}}^{(i)}}{\partial\widehat{\mathbf{d}}} \\ &= \left\{\boldsymbol{\Xi}^T\left(\boldsymbol{\Xi}\widetilde{\mathbf{d}}^{(i)} - \widetilde{\boldsymbol{\zeta}}\right)\right\}\circ\widetilde{\mathbf{d}}^{(i)}\circ\left(1 - \widetilde{\mathbf{d}}^{(i)}\right).\end{aligned} \tag{14}$$

[1]Other loss functions, such as the mean absolute error (MAE) [20], mean-squared-logarithmic error (MSLE) [21], and binary cross-entropy [8], can be applied in this problem. However, compared to the MAE, the MSE provides a more stable and unique solution, especially when the outlier does not exist in the normalized SSCV $\widetilde{\boldsymbol{\zeta}}$. Moreover, while the MSLE causes undesired peaks, a peak representing the DoA with a low signal-power level can be considered a noise element if the cross-entropy function is employed. Thus, the MSE is the most appropriate objective function for the optimization problem (10).

Given $\mathcal{G}^{(i)}$, and the predefined hyperparameters β_1 and β_s, the biased primary and secondary moments $\boldsymbol{\eta}^{(i)}$, and $\boldsymbol{\chi}^{(i)}$, and their bias-corrections $\widehat{\boldsymbol{\eta}}^{(i)}$, and $\widehat{\boldsymbol{\chi}}^{(i)}$ are subsequently updated in Steps 7–10, respectively. In Step 11, the learning parameters in $\widehat{\mathbf{d}}$ are updated using configured step-size α, and division-by-zero prevention factor ε.

Remark: The OMP method can be applied to recover the signal $\mathbf{s}(t)$ in (2), or reconstruct the spectrum $\widetilde{\mathbf{d}}$. These two schemes are named the conventional OMP (C-OMP) and modified OMP (M-OMP), respectively.

C. Computational Complexity Analysis

In Algorithm 1, the computation of SCM requires $(M^2 + M)T$ operations. Subsequently, obtaining SSCV from Step 2–4 requires $(M^2 + M)/2$. Based on (14), the computation of gradient vector in Step 7 requires $(4M\widetilde{P} + 2\widetilde{P})$ FLOPs, whereas the number of operations from Steps 8–12 is $15\widetilde{P}$. Consequently, the total complexity of GD-SSR can be approximated as $\mathcal{O}_{\mathrm{GD-SSR}} = O(M^2T + M\widetilde{P}\mathcal{I})$.

The M-MUSIC finds roots of $(M - P)$ polynomial equations [5]; thus, this yields a complexity of $O(M^4)$ [22]. The C-MUSIC requires a complexity of $O(M^3 + M^2(T + \widetilde{P}))$ [2], [8]. In addition, the C-OMP and M-OMP schemes, which recover $\overline{\mathcal{I}}$-sparse signals, require FLOPs of $O(MT\overline{\mathcal{I}}^3)$ and $O(M\overline{\mathcal{I}}^3)$, respectively. Particularly, those computational loads become $O(M^4)$, which is significantly larger than that of GD-SSR when $\overline{\mathcal{I}}$ equals $\overline{M}$. Moreover, the DeepMUSIC employs a large number of kernels to extract feature maps that also require a higher complexity than our GD-SSR [10]. Therefore, it is clear that the complexity of GD-SSR is substantially lower than those of other methods as M increases.

IV. Simulation Results and Analysis

In our simulations, an LAA with half-wavelength element spacing and effective aperture $\kappa = 10$ is used to receive the far-field signals coming from directions in a range of $\theta \in [-60^\circ, 60^\circ)$ with the angular resolution of $\rho = 0.2^\circ$. This yields $\widetilde{P} = 600$. We also assume that the LAA receives $P = 9$ signals from directions $\boldsymbol{\theta} = \{-45^\circ, -35.6^\circ, -23.2^\circ, -12.4^\circ, 8^\circ, 10^\circ, 25.2^\circ, 36.2^\circ, 52^\circ\}$ in following simulations. In addition, the parameters of GD-SSR are set as $\beta_1 = 0.9$, $\beta_2 = 0.999$, and $\varepsilon = 10^{-8}$, which are the default settings of the ADAM optimizer [19], and the step-size is chosen as $\alpha = 0.1$. For a fair comparison, only spectral-based algorithms such as C-MUSIC, DeepMUSIC, C-OMP, and M-OMP are considered for evaluation.

An example of the SSCV can be observed in Fig. 2(a) while the spectrum $\widetilde{\mathbf{d}}$ reconstructed by our GD-SSR is visualized in Fig. 2(b). Fig. 2(a) shows that the recovered SSCV by computing $\boldsymbol{\Xi}\widetilde{\mathbf{d}}$ is remarkably similar to the original one. In Fig. 2(b), it is noted that a peak value representing a target DoA θ_p is approximately equal to $\widetilde{d}_p$ obtained based on (12).

Fig. 3 demonstrates the normalized spectrum constructed by spectral-based algorithms at SNR = –10 dB. We note that the OMP schemes are susceptible to noise; thus, they are unsuitable for estimating directions in a low-SNR regime and are excluded from this simulation. It is shown that the spectrum provided by

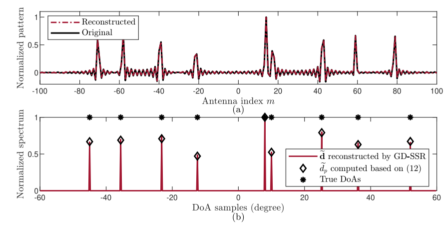

Fig. 2. (a) Original and reconstructed SSCV, i.e., $\widetilde{\boldsymbol{\zeta}}$ and $\boldsymbol{\Xi}\widetilde{\mathbf{d}}$, respectively, and (b) spectrum provided by GD-SSR, in a case that SNR = 0 dB, $\overline{M} = 100$, $P = 9$, and $\sigma^2_{s,p} \neq \sigma^2_{s,q}$, for $p \neq q$.

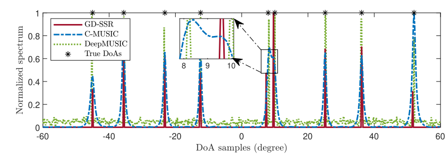

Fig. 3. Spatial spectrum comparison for $\overline{M} = 20$, and SNR = –10 dB.

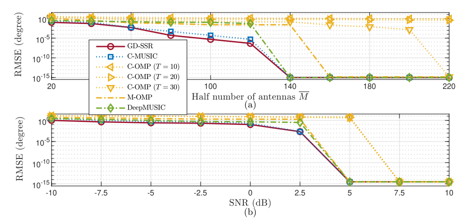

Fig. 4. RMSE performance comparison versus (a) $\overline{M}$ for SNR = 0 dB, and (b) SNR for $\overline{M} = 20$.

the GD-SSR is sharper than those of C-MUSIC and DeepMUSIC. Moreover, the GD-SSR can resolve the angular ambiguity problem better than the C-MUSIC. For example, the peaks representing 8° and 10° are merged into one in the spectrum created by the C-MUSIC scheme. The root mean-square-error (RMSE) metric with $\mathcal{W} = 500$ trials of the Monte Carlo simulation is used to evaluate the performance of our GD-SSR and other spectral-based schemes, as shown in Fig. 4. The RMSE is defined as

$$\mathrm{RMSE} = \sqrt{\frac{1}{\mathcal{W}P}\sum\nolimits_{w=1}^{\mathcal{W}}\sum\nolimits_{p=1}^{P}\left[\widehat{\theta}_p(w) - \theta_p\right]^2}. \tag{15}$$

It is shown that the proposed GD-SSR has a better performance than other schemes. In Fig. 4(a), it is observed that the GD-SSR achieves the lowest error for all values of $\overline{M}$. Fig. 4(b) also shows that the GD-SSR outperforms other methods in the low-SNR region, i.e., SNR < -5 dB.

V. Conclusion

In this letter, we have investigated a novel GD-aided DoA estimation for a symmetric LAA. The SSCV, which is created based on the property of array response, is used to perform an ℓ_2-norm optimization, and then estimate the signal direction without requiring a signal enumeration. Compared with other state-of-the-art algorithms, our proposed GD-SSR not only provides a computational complexity reduction, but also achieves better estimation performance, especially in a low-SNR region, while handling manifold ambiguity problems.

References

[1] Y. Zeng and R. Zhang, "Millimeter wave MIMO with lens antenna array: A new path division multiplexing paradigm," *IEEE Trans. Commun.*, vol. 64, no. 4, pp. 1557–1571, Apr. 2016.

[2] D. T. Hoang and K. Lee, "Deep learning-aided signal enumeration for lens antenna array," *IEEE Access*, vol. 10, pp. 123835–123846, 2022.

[3] R. Schmidt, "Multiple emitter location and signal parameter estimation," *IEEE Trans. Antennas Propag.*, vol. 34, no. 3, pp. 276–280, Mar. 1986.

[4] B. D. Rao and K. S. Hari, "Performance analysis of Root-MUSIC," *IEEE Trans. Signal Process.*, vol. 37, no. 12, pp. 1939–1949, Dec. 1989.

[5] Z. Ni, Y. Luo, M. Motani, and C. Li, "DoA estimation for lens antenna array via root-MUSIC, outlier detection, and clustering," *IEEE Access*, vol. 8, pp. 199187–199196, 2020.

[6] J. A. Tropp and A. C. Gilbert, "Signal recovery from random measurements via orthogonal matching pursuit," *IEEE Trans. Inf. Theory*, vol. 53, no. 12, pp. 4655–4666, Dec. 2007.

[7] K. Aghababaiyan, V. Shah-Mansouri, and B. Maham, "High-precision OMP-based direction of arrival estimation scheme for hybrid non-uniform array," *IEEE Commun. Lett.*, vol. 24, no. 2, pp. 354–357, Feb. 2020.

[8] D. T. Hoang and K. Lee, "Coherent signal enumeration based on deep learning and the FTMR algorithm," in *Proc. IEEE Int. Conf. Commun.*, Seoul, South Korea, 2022, pp. 5098–5103.

[9] A. M. Elbir, "DeepMUSIC: Multiple signal classification via deep learning," *IEEE Sens. Lett.*, vol. 4, no. 4, pp. 1–4, Apr. 2020.

[10] D. T. Hoang and K. Lee, "Deep learning-aided coherent direction-of-arrival estimation with the FTMR algorithm," *IEEE Trans. Signal Process.*, vol. 70, pp. 1118–1130, 2022.

[11] Y. Arjoune, N. Kaabouch, H. El Ghazi, and A. Tamtaoui, "Compressive sensing: Performance comparison of sparse recovery algorithms," in *Proc. IEEE 7th Annu. Comput. Commun. Workshop Conf.*, 2017, pp. 1–7.

[12] A. Imakura and Y. Yamamoto, "Efficient implementations of the modified Gram–Schmidt orthogonalization with a non-standard inner product," *Jpn. J. Ind. Appl. Math.*, vol. 36, no. 2, pp. 619–641, Mar. 2019.

[13] Y. Kase, T. Nishimura, T. Ohgane, Y. Ogawa, D. Kitayama, and Y. Kishiyama, "DOA estimation of two targets with deep learning," in *Proc. 15th Workshop Positioning Navigation Commun.*, 2018, pp. 1–5.

[14] Z.-M. Liu, C. Zhang, and S. Y. Philip, "Direction-of-arrival estimation based on deep neural networks with robustness to array imperfections," *IEEE Trans. Antennas Propag.*, vol. 66, no. 12, pp. 7315–7327, Dec. 2018.

[15] A. M. Ahmed, O. Eissa, and A. Sezgin, "Deep autoencoders for DOA estimation of coherent sources using imperfect antenna array," in *Proc. 3rd Int. Workshop Mobile Terahertz Syst.*, 2020, pp. 1–5.

[16] Y. Cao, T. Lv, Z. Lin, P. Huang, and F. Lin, "Complex ResNet aided DoA estimation for near-field MIMO systems," *IEEE Trans. Veh. Technol.*, vol. 69, no. 10, pp. 11139–11151, Oct. 2020.

[17] R. Hunger, "Floating point Operations in Matrix-Vector Calculus," Inst. Circuit Theory Signal Processing, Munich Univ. Technol., Munich, Germany, Tech. Rep. 2007, 2005.

[18] A. V. Oppenheim, J. Buck, M. Daniel, A. S. Willsky, S. H. Nawab, and A. Singer, *Signals and Systems*. London, U.K.: Pearson Educación, 1997.

[19] D. P. Kingma and J. Ba, "Adam: A method for stochastic optimization," in *Proc. 3rd Int. Conf. Learn. Representation*, 2014, pp. 115.

[20] A. Botchkarev, "A new typology design of performance metrics to measure errors in machine learning regression algorithms," *Interdiscipl. J. Inf., Knowl. Manage.*, vol. 14, pp. 045–076, Jan. 2019.

[21] C. Chrysostomou, "The effect of loss functions on denoising and reconstructing sinograms based on deep learning methodologies," in *Proc. Nucl. Sci. Symp. Med. Imag. Conf.*, 2021, pp. 1–4.

[22] E. Gentilho, P. R. Scalassara, and T. Abrão, "Direction-of-arrival estimation methods: A performance-complexity tradeoff perspective," *J. Signal Process. Syst.*, vol. 92, no. 2, pp. 239–256, Feb. 2020.